Article

Stability of Luminescent Trivalent Cerium in Silica Host Glasses Modified by Boron and Phosphorus

Carmen Canevali, Mariachiara Mattoni, Franca Morazzoni, Roberto Scotti, Mariano Casu, Anna Musinu, Radenka Krsmanovic, Stefano Polizzi, Adolfo Speghini, and Marco Bettinelli

J. Am. Chem. Soc., **2005**, 127 (42), 14681-14691• DOI: 10.1021/ja052502o • Publication Date (Web): 01 October 2005

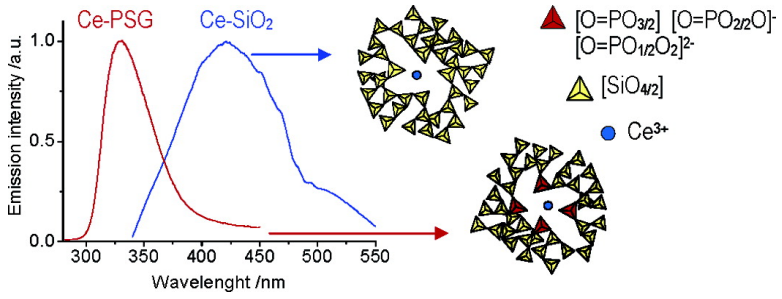

More About This Article

Additional resources and features associated with this article are available within the HTML version:

- Supporting Information
- Links to the 5 articles that cite this article, as of the time of this article download
- Access to high resolution figures
- Links to articles and content related to this article
- Copyright permission to reproduce figures and/or text from this article

View the Full Text HTML

J|A|C|S
ARTICLES
Published on Web 10/01/2005

Stability of Luminescent Trivalent Cerium in Silica Host Glasses Modified by Boron and Phosphorus

Carmen Canevali,[†] Mariachiara Mattoni,[†] Franca Morazzoni,[†] Roberto Scotti,*[,†] Mariano Casu,[‡] Anna Musinu,[‡] Radenka Krsmanovic,[§] Stefano Polizzi,[§] Adolfo Speghini,[||] and Marco Bettinelli[||]

Contribution from the Dipartimento di Scienza dei Materiali, Università di Milano-Bicocca, INSTM, via Cozzi 53, 20125 Milano, Dipartimento di Scienze Chimiche, Università di Cagliari, INSTM, SS554 Bivio per Sestu, 09042 Monserrato (CA), Dipartimento di Chimica Fisica, Università Ca' Foscari, INSTM, via Torino 155/b, 30172 Venezia-Mestre, and Dipartimento di Scientifico e Tecnologico, Università di Verona, INSTM, strada le Grazie 15, 37134 Verona, Italy

Received April 18, 2005; E-mail: Roberto.Scotti@unimib.it

Abstract: Ce-doped borosilicate (BSG), phosphosilicate (PSG), and borophosphosilicate (BPSG) glasses (B:P:Si molar ratios 8:0:92, 0:8:92, and 8:8:84; Ce:Si molar ratio 1×10^{-4} to 1×10^{-2}) were prepared by the sol−gel method. High-resolution transmission electron microscopy (HRTEM), ^{31}P, ^{29}Si, and ^{11}B magic angle spinning nuclear magnetic resonance (MAS NMR), electron paramagnetic resonance (EPR), and UV−vis absorption investigations demonstrated that, in PSG and BPSG, Ce^{3+} ions interact with phosphoryl, $[O{=}PO_{3/2}]$, metaphosphate, $[O{=}PO_{2/\ 2}O]^-$, and pyrophosphate, $[O{=}PO_{1/2}O_2]^{2-}$, groups, linked to a silica network. This inhibits both CeO_2 segregation and oxidation of isolated Ce^{3+} ions to Ce^{4+}, up to Ce:Si = 5×10^{-3}. In BSG, neither trigonal $[BO_{3/2}]$ nor tetrahedral $[BO_{4/2}]^-$ boron units coordinate cerium; thus, Ce^{3+} oxidation occurs even at Ce:Si = 1×10^{-4}, as in pure silica glass (SG). The homogeneous rare-earth dispersion in the host matrix and the stabilization of the Ce^{3+} oxidation state enhanced the intensity of the photoluminescence emission in PSG and BPSG with respect to BSG and SG. The energy of the Ce^{3+} emission band in PSG and BPSG matrixes agrees with the phosphate environment of the rare earth.

Introduction

Ce-doped crystalline compounds have received great interest owing to the rare-earth (RE) luminescence properties.[1,2] In fact, trivalent cerium has a broad emission band in the UV−vis region due to the allowed 5d−4f transition. As the energies of the 5d levels are strongly affected by the crystal field around Ce^{3+}, significant shifts of the emission energy occur in different host crystalline matrixes.[3] Notable properties of luminescent Ce^{3+} ions are the fast 5d−4f decay time and the relatively high light output, which make Ce^{3+}-containing solids promising materials in several applications such as phosphors for cathodoluminescence,[4] scintillators for applications in high-energy physics[5−7] and for the detection of X-rays, γ-rays, or neutrons,[8−12] and tunable solid-state lasers operating in the near-UV, violet, and blue regions.[13−18]

The luminescence yield is unfavorably affected by Ce^{3+} aggregation phenomena. When the RE concentration increases, the ion distance becomes comparable to the critical distance, at which the radiative decay probability equals the energy transfer rate, leading to nonradiative processes[19,20] and, therefore, to

[†] Università di Milano-Bicocca.
[‡] Università di Cagliari.
[§] Università Ca' Foscari.
[||] Università di Verona.

(1) van Loaf, E. V. D.; Dorenbos, P.; Van Eijk, C. W. E.; Kramer, K.; Guide, H. U. *Appl. Phys. Lett.* **2000**, *77*, 1467.
(2) van Loef, E. V. D.; Dorenbos, P.; Van Eijk, C. W. E.; Krämer, K.; Güdel, H. U. *Appl. Phys. Lett.* **2001**, *79*, 1573.
(3) Dorenbos, P.; Pierron, L.; Dinca, L.; Van Eijk, C. W. E.; Kahn-Harari, A.; Viana, B. *J. Phys.: Condens. Matter* **2003**, *15*, 511.
(4) Reisfeld, R.; Jørgesen, C. K. In *Heavy scintillators for scientific and industrial applications*; De Notaristefani, F., Lecoy, P., Schneegans, M., Eds.; Frontieres: Gif-sur-Yvette, France, 1993; p 155G.
(5) Dafinei, I.; et al. *Nucl. Instrum. Methods Phys. Res., A* **1996**, *380*, 524.
(6) Martini, M.; Meinardi, F.; Vedda, A.; Dafinei, I.; Lecoq, P.; Nikl, M. *Nucl. Instrum. Methods Phys. Res., B* **1996**, *116*, 116.
(7) Dujardin, C.; Pedrini, C.; Moysan, M.; Carreé, J. Y.; Mazé, G.; Jiary, J.; Zhang, G.; Poulain, M. In *Proceedings of the International Conference on Inorganic Scintillators and their Applications (SCINT '97)*, Shanghai, People's Republic of China, Sept 22−25, 1997; Zhiwen, Y., Pejun, L., Xigi, F., Zhilin, X., Eds.; CAS Shanghai Branch Press: Shanghai, 1997; p 376.
(8) Zanella, G.; Zannoni, R.; Dall'Igna, R.; Locardi, B.; Polato, P.; Bettinelli, M.; Marigo A. *Nucl. Instrum. Methods Phys. Res., A* **1994**, *345*, 198.
(9) Zanella, G.; Zannoni, R.; Dall'Igna, R.; Polato, P.; Bettinelli M. *Nucl. Instrum. Methods Phys. Res., A* **1995**, *359*, 547.
(10) Baccaro, S.; Dall'Igna, R.; Fabeni, P.; Martini, M.; Mares, J. A.; Meinardi, F.; Nikl, M.; Nitsch, K.; Pazzi, G. P.; Polato, P.; Vedda, A.; Zanella, G.; Zannoni, R. *J. Lumin.* **2000**, *87*, 673.
(11) Nikl, M.; Nitsch, K.; Mihokova, E.; Solovieva, N.; Mares, J. A.; Fabeni, P.; Pazzi, G. P.; Martini, M.; Vedda, A.; Baccaro, S. *Appl. Phys. Lett.* **2000**, *77*, 2159.
(12) van Eijk, C. W. E. *Nucl. Instrum. Methods Phys. Res., A* **1997**, *392*, 285.
(13) Okada, F.; Togata, S.; Otho, K.; Koda, S. *J. Appl. Phys.* **1994**, *75*, 49.
(14) Marshall, C. D.; Speth, J. D.; Payne, S. A. *J. Opt. Soc. Am. B* **1994**, *11*, 2054.
(15) Kucuk, A.; Clare, A. G. *Opt. Mater.* **1999**, *13*, 279.
(16) Murata T.; Sato M.; Yoshida H.; Morinaga K. *J. Non-Cryst. Solids* **2005**, *351*, 312.
(17) Lim, K. S.; Hamilton, D. S. *J. Opt. Soc. Am. B* **1989**, *6*, 1401.
(18) La Roche, M.; Girard, S.; Moncorge, R.; Bettinelli, M.; Abdulsabirov, R.; Semashko, V. *Opt. Mater.* **2003**, *22*, 147.
(19) Auzel, F.; Goldner, P. *Opt. Mater.* **2001**, *16*, 93.

concentration quenching. Besides, another process leading to the quenching of Ce^{3+} luminescence is the oxidation to nonluminescent Ce^{4+}.

Glass hosts were proposed as an alternative to crystalline ones[5−11] due to their attractive characteristics such as low cost, flexible shape, and possible employment in fiber technology. The main drawback is the low efficiency of energy transfer from the host glass matrix to the emission centers. This results in low light output,[5] caused by the presence of point defects and OH groups, which provide nonradiative recombination channels.

Ce-containing luminescent glasses of different compositions have been conventionally prepared by quenching of oxide melts.[5−11,18] The sol−gel procedure has been more recently proposed as an alternative route to synthesize high-purity luminescent glasses embedding controlled amounts of rare-earth activator ions.[21−25] This technique allows the formation of the glass network at room temperature as a result of hydrolysis and condensation reactions of the precursors mixed in solution. The subsequent glass densification process is performed, after gelation, at temperatures lower than in melting methods, in principle avoiding or lowering the probability that point defects arise in the host glass matrix. Recently, we succeeded in preparing Ce-doped silica glasses[26−29] by the sol−gel method. These materials showed promising radioluminescence efficiency, depending on the RE concentration[26] and on the densification temperature.[30,31] However, significant luminescence quenching occurred in glass samples with a Ce:Si molar ratio higher than 1×10^{-3}, as Ce^{3+} oxidized and segregated as nonluminescent nanosized CeO_2.[32]

To embed Ce^{3+} ions in a glass matrix, avoiding CeO_2 segregation, we propose to modify the silica matrix with P and B glass formers. Borate and phosphate glasses have been diffusely studied as host matrixes for different rare earths, and their influence on the optical properties has been deeply investigated.[33−35] Here B and P are expected to induce local distortions in the silica network and to generate structural defects resulting in a less textured glass structure, as indicated by the lower glass transition and flow temperatures.[36] Consequently, Ce^{3+} centers should be embedded in the host matrix and possibly bind to B- and P-related defects, thus increasing their relative distance and having weaker interaction between them. As a matter of fact, our recent investigation[37] on monolithic borophosphosilicate glasses demonstrated that nonbridging and bridging oxygens of B and P units linked to a silica network play a major role in trapping electron holes (h^+) under X-ray irradiation. This ability suggests that the same oxygen atoms could, in principle, preferentially interact with the positively charged Ce^{3+} ions.

The present work focused on obtaining borosilicate (BSG), phosphosilicate (PSG), and borophosphosilicate (BPSG) Ce-doped glasses (Ce:Si molar ratio 1×10^{-4} to 1×10^{-2}) by sol−gel synthesis, with the aim of improving the Ce^{3+} dispersion in the host glass matrix and of lowering the oxidative CeO_2 segregation observed in silica glass (SG).[32] The BSG, PSG, and BPSG nominal compositions, respectively, 8:0:92, 0:8:92, and 8:8:84 B:P:Si molar ratios, were chosen among those reported in the previous investigation.[37]

The occurrence of the crystalline CeO_2 phase in BSG, PSG, and BPSG was investigated by high-resolution transmission electron microscopy (HRTEM). To describe the structural glass modifications caused by RE embedding and to identify the binding sites responsible for the RE coordination, electron paramagnetic resonance (EPR), magic angle spinning nuclear magnetic resonance (MAS NMR), UV−vis absorption, and photoluminescence measurements were performed. EPR resonance lines of phosphorus oxygen hole centers (POHCs) and boron oxygen hole centers (BOHCs) in the X-ray-irradiated Ce-doped glasses allowed us to check the RE interaction with B- and P-related defects. Finally, photoluminescence properties of the material were correlated to the ability of the glasses in stabilizing the RE trivalent state.

Experimental Section

Ce-doped SGs (Ce:Si molar ratio in the range 1×10^{-4} to 1×10^{-2}) were prepared by the sol−gel method with a procedure reported elsewhere,[26] using tetraethoxysilane (TEOS) and $Ce(NO_3)_3 \cdot 6H_2O$ as precursors. An ethanol solution of TEOS was mixed under stirring with a suitable amount of $Ce(NO_3)_3 \cdot 6H_2O$ in an ethanol−water solution. TEOS:H_2O:EtOH volume ratios were 1:0.6:3; the H_2O:TEOS molar ratio was 7.4:1. Gelation occurred at 35 °C in 10−20 days, and transparent xerogels were obtained by slowly drying the alcogel (7−15 days at 35 °C). Xerogels were subsequently densified to glasses by thermal treatment up to 1323 K, using a flowing oxygen atmosphere up to 723 K and then reduced pressure (1.33 Pa) up to 1323 K.

Ce-doped BSG, PSG, and BPSG (Ce:Si molar ratio in the range 1×10^{-4} to 1×10^{-2}) were prepared by the sol−gel method using tetramethoxysilane (TMOS), trimethyl phosphite (TMP), trimethyl borate (TMB), and $Ce(NO_3)_3 \cdot 6H_2O$ as precursors (Scheme 1). TMOS was partially hydrolyzed in methanol solution under stirring at 45 °C for 1 h (H_2O:TMOS molar ratio 2:1) before addition of a suitable amount of TMP and TMB (B:Si molar ratio 8:92 for BSG, P:Si molar ratio 8:92 for PSG, and B:P:Si molar ratio 8:8:84 for BPSG) and a second amount of water (H_2O:TMOS molar ratio 2:1) acidified with HNO_3 (10^{-3} M). The solution was continuously stirred at 45 °C for 4 h, and then a methanol solution of $Ce(NO_3)_3 \cdot 6H_2O$ was added. Gelation occurred at 35 °C in 3−5 days, and afterward, transparent xerogels were obtained by slowly drying the alcogels (∼15 days at 35 °C). Xerogels were densified to glasses by thermal treatment up to 973 K, by alternating flowing oxygen (17 h) and reduced pressure (7 h) every

(20) Blasse, G.; Grabmeier, B. C. *Luminescent Materials*; Springer-Verlag: Berlin, 1994.
(21) Weiping, C.; Ye, Z.; Lide, Z. *J. Phys.: Condens. Matter* **1998**, *10*, L473.
(22) Malashkevich, G. E.; Melnichenko, I. M.; Poddenezhny, E. N.; Boiko, A. A. *J. Non-Cryst. Solids* **1999**, *260*, 141.
(23) Reisfeld, R.; Patra, A.; Panczer, G.; Gaft, M. *Opt. Mater.* **1999**, *13*, 81.
(24) Itoh, K.; Kamata, N.; Shimazu, T.; Satoh, C.; Tonooka, K.; Yamada, K. *J. Lumin.* **2000**, *87−89*, 676.
(25) Tonooka, K.; Nishimura, O. *J. Lumin.* **2000**, *87−89*, 679.
(26) Vedda, A.; Baraldi, A.; Canevali, C.; Capelletti, R.; Chiodini, N.; Francini, R.; Martini, M.; Morazzoni, F.; Nikl, M.; Scotti, R.; Spinolo, G. *Nucl. Instrum. Methods Phys. Res., A* **2002**, *486*, 259.
(27) Chiodini, N.; Fasoli, M.; Martini, M.; Rosetta, E.; Spinolo, G.; Vedda, A.; Nikl, M.; Solovieva, N.; Baraldi, A.; Capelletti, R. *Appl. Phys. Lett.* **2002**, *81*, 4375.
(28) Chiodini, N.; Fasoli, M.; Martini, M.; Morazzoni, M.; Rosetta, E.; Scotti, R.; Spinolo, G.; Vedda, A.; Nikl, M.; Solovieva, N.; Baraldi, A.; Capelletti, R.; Francini, R. *Radiat. Eff. Defects Solids* **2003**, *158*, 463.
(29) Chiodini, N.; Vedda, A.; Baraldi, A.; Martini, M.; Nikl, M.; Scotti, R.; Spinolo, G. PCT Int. Appl. WO 2003048058, A1, 20030612, 2003.
(30) Baraldi, A.; Capelletti, R.; Chiodini, N.; Mora, C.; Scotti, R.; Uccellini, E.; Vedda, A. *Nucl. Instrum. Methods Phys. Res., A* **2002**, *486*, 408.
(31) Baraldi, A.; Capelletti, R.; Chiodini, N.; Oppici, C.; Scotti, R.; Vedda, A. *Radiat. Eff. Defects Solids* **2003**, *157*, 1139.
(32) Di Martino, D.; Vedda, A.; Angella, G.; Catti, M.; Cazzini, E.; Chiodini, N.; Morazzoni, F.; Spinolo, G. *Chem. Mater.* **2004**, *16*, 3352.
(33) Izumitani, T.; Toratani, H.; Kuroda, H. *J. Non-Cryst. Solids* **1982**, *47*, 87.
(34) Takebe, H.; Morinaga, K.; Izumitani, T. *J. Non-Cryst. Solids* **1994**, *178*, 58.
(35) Peng, B.; Izumitani, T. *Opt. Mater.* **1995**, *4*, 797.
(36) Kim, J. Y.; Kumpta, P. N. *J. Phys. Chem. B* **1998**, *102*, 5744.
(37) Canevali, C.; Scotti R.; Vedda, A.; Mattoni, M.; Morazzoni, F.; Armelao, L.; Barreca, D.; Bottaro, G. *Chem. Mater.* **2004**, *16*, 315.

Scheme 1. Synthesis Procedure of Ce-Doped BSG, PSG, and BPSG

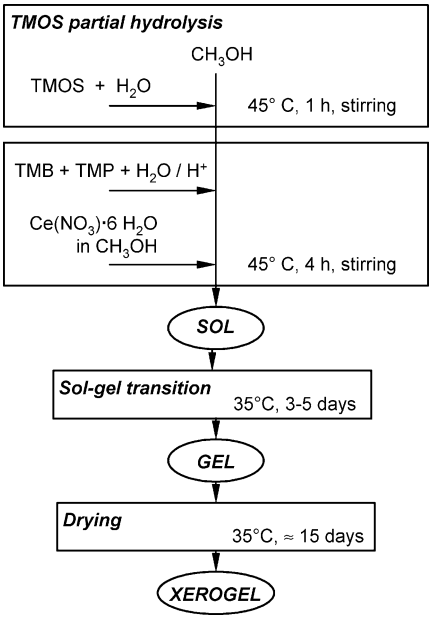

50 K up to 723 K and operating under reduced pressure (1.33 Pa) up to 973 K.

Transparent monolithic disks with a diameter of ∼2.5 cm and thickness of ∼0.2 cm were obtained. At 973 K xerogels are fully densified as demonstrated by the Raman and FTIR analysis.[37]

As concerns the actual P and B glass composition, determined as reported in a previous investigation,[37] no loss of P occurs whereas the B content is ∼30% less than the nominal amount. Boron loss was already observed by other authors[25,38] during the xerogel thermal treatment, and it was attributed to volatilization of boron compounds. The analysis of cerium content was performed by inductively coupled plasma (ICP) emission spectroscopy and demonstrated that no cerium loss occurs during synthesis and thermal treatment. Samples for the ICP emission spectroscopy analysis were prepared in a Teflon crucible by dissolving the glass in a mixture (1:3 v/v) of HF (48% w/w in water, Aldrich) and $HClO_4$ (70% w/w in water, Aldrich). The solution was then dried and the powder dissolved again in HCl (37% w/w in water, Aldrich), diluting with water to a suitable concentration for the analysis. Drying procedures were performed on a heating plate placed in an appropriately rated fume hood, coated with HF-resistant material.

HRTEM analysis was performed at 300 kV using a JEOL 3010 apparatus with a high-resolution pole piece (0.17 nm point-to-point resolution), equipped with a Gatan slow-scan 794 CCD camera. The elemental composition was determined by an Oxford Instruments EDS microanalysis detector (model 6636). Glass samples were ground in an agate mortar, and the resulting fine powder was suspended in 2-propanol. A 5 μL drop of this suspension was deposited on a holey carbon film supported on a 3 mm copper grid for TEM investigation.

Ce^{3+} EPR spectra were recorded at 4.2 K on monolithic glass fragments by a Bruker EMX spectrometer equipped with an Oxford cryostat operating in the 4.2−373 K temperature range. The *g* values were measured by using diphenylpicrylhydrazyl (DPPH) as the standard, and the amounts of paramagnetic species were obtained by double integration of the resonance line areas, taking as reference the Bruker weak pitch ($9.7 \times 10^{12} \pm 5\%$ spin/cm). EPR investigation of BOHC and POHC paramagnetic defects was performed at 298 K on monolithic glass fragments, before and immediately after X-ray irradiation with a dose of about 10^3 Gy. Irradiation was performed at room temperature by an X-ray tube (Machlett OEG 50) operating at 30 kV. The experimental spectra were fitted by the Bruker Simfonia simulation program.

High-resolution NMR experiments were performed at room temperature by a Varian UNITY INOVA spectrometer equipped with a 9.39 T wide-bore Oxford magnet and having an MAS probe with 4 mm Si_3N_4 rotors. The ^{29}Si MAS spectra were collected at 79.4 MHz, at a spinning rate of 6 kHz, with a recycle time of 500 s, 4.5 μs pulse lengths (45° tip angle), a 40 kHz bandwidth, and 200 scans in each experiment. The CPMAS spectra were collected with a recycle time of 4 s and a contact time as indicated in the Results and Discussion. The ^{29}Si chemical shift was referred to that of tetramethylsilane. The ^{11}B MAS spectra were collected at 128.3 MHz, at a spinning rate of 12 kHz, with a recycle time of 4 ms, a high-power 0.6 μs pulse length (15° tip angle) to ensure quantitative observation of the boron types, and a 50 kHz bandwidth in each experiment. A 10 Hz exponential broadening was applied before Fourier transformation. The ^{11}B chemical shift was referred to that of 1 M aqueous boric acid set at 19.5 ppm. The ^{31}P MAS spectra were collected at 161.9 MHz, at a spinning rate of 10 kHz, which was sufficient to lower the intensity of spinning sidebands, with a recycle delay of 100 s, 7 μs pulse lengths (90° tip angle), and a 40 kHz bandwidth in each experiment. A 50 Hz exponential broadening was applied before Fourier transformation. The ^{31}P chemical shift was referred to an 85% w/w aqueous solution of phosphoric acid.

The species distributions in ^{29}Si and ^{31}P MAS experiments were obtained by a nonlinear fitting of the NMR spectra to individual Gaussians by means of the Origin 4.1 program from Microcal Software. In the fitting procedure, the position, line width, and intensity were varied to find the best fit curve to the experimental spectra. The contribution to the intensity of the spinning sidebands in the ^{31}P spectra was taken into account in the evaluation of species distribution. The central transition line shape of the ^{11}B MAS spectra was simulated with the WSOLIDS[39] program using infinite spinning speed approximation.

The absorption spectra in the UV−vis range were measured using a Uvikon 941 UV−vis double-beam spectrophotometer with a spectral resolution of 0.5 nm. The UV−vis luminescence spectra were measured with a conventional Jasco FP-777 spectrofluorimeter with a spectral resolution of 1.5 nm. The luminescence decay curves in the UV region were measured by exciting at 290 mm with the second harmonic of a dye laser (using Rodamine 6G as the dye) pumped with the second harmonic (532 nm) of a pulsed Nd:YAG laser. A fiber optic probe was employed to collect the emission. The signal was analyzed by a 1/2 m monochromator equipped with a 150 lines/mm grating. A GaAs photomultiplier and a digital oscilloscope were used to measure the emission decay curves. The decay times were obtained from the emission decay curves using a deconvolution procedure which takes into account the shape and the duration of the excitation pulse. All the optical spectroscopic measurements were performed at room temperature.

Results and Discussion

High-Resolution Transmission Electron Microscopy. The microstructural characterization of Ce-doped SG, BSG, PSG, and BPSG with different Ce contents was performed by HRTEM. Ce-doped SG samples with a Ce:Si molar ratio $>5 \times 10^{-4}$ showed segregation of nanocrystalline spherical CeO_2 particles, while samples with lower molar ratios were amorphous. Figure 1 reports some representative HRTEM micrographs of glasses with different Ce contents (Ce:Si molar ratios 7×10^{-4} and 1×10^{-2}). The presence of the CeO_2 phase was assessed by the lattice plane distance of 3.1 Å identified in the

(38) Yamanaka, S.; Akagi, J.; Hattori, M. *J.Non-Cryst. Solids* **1985**, *70*, 279.

(39) Eichele K.; Wasylishen, E. R. WSOLIDS NMR Simulation Package, 2001. See http://ramsey.chem.ualberta.ca/programs.html and http://casgm3.anorg.chemie.uni-tuebingen.de/klaus/soft/index.html.

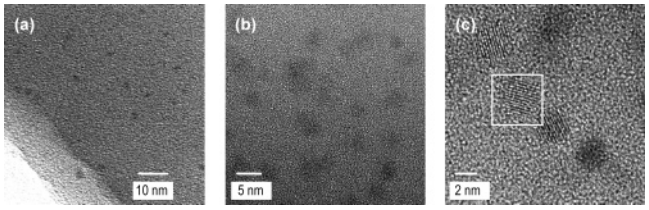

Figure 1. HRTEM images of Ce-doped SG: (a) Ce:Si = 7×10^{-4} molar ratio; (b) Ce:Si = 1×10^{-2} molar ratio; (c) the (111) planes of CeO_2 nanocrystals in a Ce:Si = 1×10^{-2} molar ratio glass.

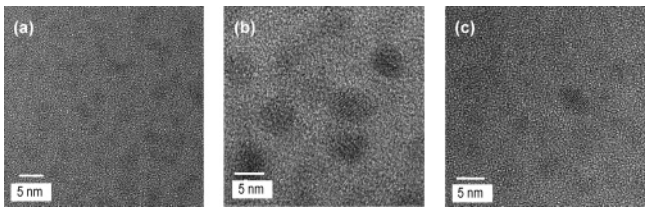

Figure 2. HRTEM images of (a) Ce-doped BSG, (b) Ce-doped PSG, and (c) Ce-doped BPSG with a Ce:Si = 1×10^{-2} molar ratio.

sample with a Ce:Si molar ratio of 1×10^{-2}, which corresponds to that of the (111) ceria planes, 3.1234 Å.[40] The size of CeO_2 particles increases with increasing RE content, from ~2 nm for Ce:Si = 7×10^{-4} to ~5 nm for Ce:Si = 1×10^{-2}. Ce-doped BSG, PSG, and BPSG appeared amorphous up to Ce:Si = 5×10^{-3}, and CeO_2 nanoparticle segregation occurred only at the highest investigated RE content, Ce:Si = 1×10^{-2}, more than 10 times greater than in SG (Figure 2), even if it cannot be excluded that at lower concentrations CeO_2 particles were too small to be detected by TEM. As the elemental analyses demonstrated that no cerium was lost during sample preparation, it appears that the inclusion of B and P glass formers into the silica network strongly inhibited the tendency of CeO_2 to segregate, favoring the RE dispersion.

Absorption and Luminescence Spectroscopy. The absorption spectra of selected glasses in the UV−vis region are shown in Figure 3. Ce-doped SG (Ce:Si = 2×10^{-4} molar ratio) shows a broad and structureless band peaking at ~260 nm (Figure 3a). The absorption can be attributed to Ce^{4+} charge transfer transition, in analogy to that reported for differently prepared Ce-doped silica glasses.[41]

Since HRTEM micrographs demonstrated that SG samples with a Ce:Si molar ratio $< 5 \times 10^{-4}$ were amorphous and did not contain CeO_2 nanoparticles, we are forced to assume that a number of Ce^{4+} ions are homogeneously dispersed in the SG matrix, most probably due to oxidation during the thermal treatment. The same behavior was observed for Ce-doped BSG (Ce:Si = 1×10^{-3} molar ratio, not shown in Figure 3).

The spectra of the Ce-doped PSG and BPSG glasses (Ce:Si = 1×10^{-3} molar ratio) were quite different (Figure 3b,c), both clearly showing five broad bands with the strongest one peaking at ~290 nm. The bands can be assigned to the allowed transitions from the $^2F_{5/2}$ ground level to the $^2D(5d)$ excited levels of the Ce^{3+} ions.[42,43] The occurrence of five components[41,44] is due to the $^2D(5d)$ level splitting of Ce^{3+} ion in the

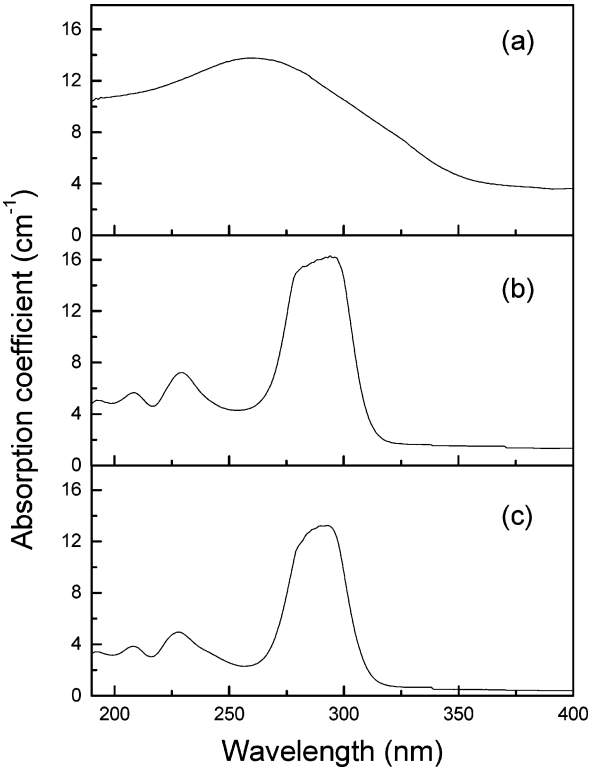

Figure 3. Room-temperature absorption spectra of the (a) Ce-doped SG (Ce:Si = 2×10^{-4} molar ratio), (b) Ce-doped PSG (Ce:Si = 1×10^{-3} molar ratio), and (c) Ce-doped BPSG (Ce:Si = 1×10^{-3} molar ratio).

ligand field of the host glass. In PSG and BPSG Ce^{4+} ions are present, if any, at a very low concentration.

Luminescence and excitation spectra of Ce-doped SG (Ce:Si = 2×10^{-4} molar ratio) show broad bands, peaking at about 420 and 325 nm, respectively (Figure 4a), similar to those reported in the literature for Ce-doped silica glasses.[41,45,46] The broad luminescence band is assigned to 5d−4f transition of Ce^{3+}. Luminescence and excitation spectra of Ce-doped BSG glasses (Ce:Si = 5×10^{-3} molar ratio) resembled those of Ce-doped SG (Figure 4b). The emission band peaks at ~410 nm, whereas the excitation band appears at ~320 nm. Both bands are slightly shifted toward lower wavelengths with respect to the corresponding emission and excitation bands of Ce-doped SG.

Figure 5 shows the emission and excitation spectra of Ce-doped BPSG at different RE concentrations. The emission and excitation spectra of Ce-doped PSG (not shown) showed quite similar peaks with slight differences in the peak wavelength.

The energy of Ce^{3+} emissions was very different in PSG and BPSG with respect to SG and BSG. In fact, the emission spectra of Ce-doped PSG and BPSG up to a Ce:Si = 1×10^{-3} molar ratio showed broad asymmetric bands peaking, respectively, at ~337 and 330 nm, values very similar to those reported for Ce^{3+} in phosphate glasses.[11,41] As the Ce concentration in the host glass increased, the peak of the emission band shifted toward higher wavelengths. In particular, for the sample with a

(40) CDD Powder Diffraction File, Card No. 34-0394, International Centre for Diffraction Data, Newton Square, PA.
(41) Ishii, Y.; Arai, K.; Namikawa, H.; Tanaka, M.; Negishi, A.; Handa, T. *J. Am. Ceram. Soc.* **1987**, *70*, 72.
(42) Svetashev, A. G.; Tsvirko, M. P. *Opt. Spektrosk.* **1985**, *56*, 515.
(43) Dorembos, P.; Pierron, L.; Dinca, L.; van Eijk, C. W. E.; Kahn-Harari, A.; Viana, B. *J. Phys.: Condens. Matter* **2003**, *15*, 511.
(44) Reisfeld, R.; Harmodaly, J. *Proc. Rare Earth Res. Conf., 9th* **1971**, *1*, 123.
(45) Malashkevich, G. E.; Poddenezhny, E. N.; Melnichencko, I. M.; Boiko, A. A. *J. Non-Cryst. Solids* **1995**, *188*, 107.
(46) Malashkevich, G. E.; Melnichencko, I. M.; Poddenezhny, E. N.; Boiko, A. A. *J. Non-Cryst. Solids* **1999**, *260*, 141.

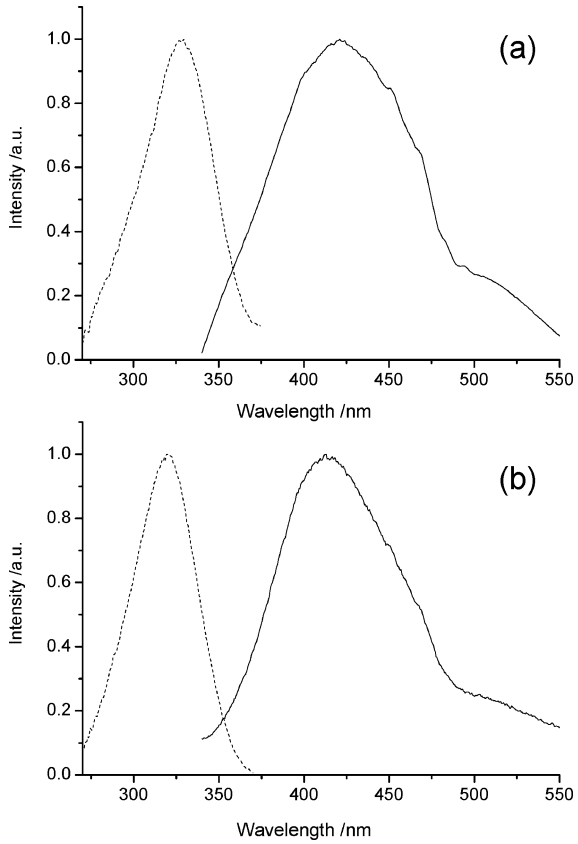

Figure 4. (a) Room-temperature emission ($\lambda_{exc} = 330$ nm, solid line) and excitation ($\lambda_{em} = 422$ nm, dashed line) spectra of Ce-doped SG (Ce:Si = 2×10^{-4} molar ratio). (b) Room-temperature emission ($\lambda_{exc} = 320$ nm, solid line) and excitation ($\lambda_{em} = 410$ nm, dashed line) spectra of Ce-doped BSG (Ce:Si = 1×10^{-3} molar ratio). Spectral intensities are normalized.

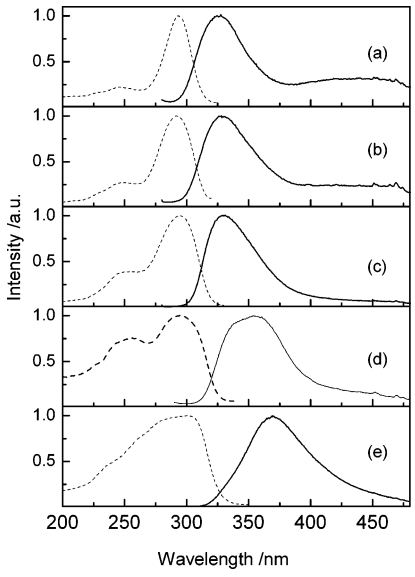

Figure 5. Room-temperature emission ($\lambda_{exc} = 250$ nm, solid line) and excitation ($\lambda_{em} = 370$ nm, dashed line) spectra of Ce-doped BPSG glasses with different Ce:Si molar ratios: (a) 1×10^{-4}; (b) 5×10^{-4}; (c) 1×10^{-3}; (d) 5×10^{-3}; (e) 1×10^{-2}. Spectral intensities are normalized.

Ce:Si molar ratio of 1×10^{-2}, the luminescence band peaked at ~370 nm with a shoulder at about 330 nm.

To estimate the Ce^{3+} relative emission intensities in different matrixes, the luminescence spectra were measured in closely similar experimental conditions and with the same excitation wavelength ($\lambda_{exc} = 282$ nm). The emission intensities were obtained by integrating the Ce^{3+} emission bands and normalizing them with respect to the thickness of the samples and the absorption coefficients at the excitation wavelength. The absorption coefficients were obtained from the corresponding absorption spectra. The insertion of P into the silica network significantly increased the emission intensity of Ce^{3+}; in fact, Ce-doped PSG and BPSG samples always showed stronger emission intensities than Ce-doped SG with the same RE content. Ce-doped BSG had weaker or similar emission with respect to Ce-doped SG. As an example, the ratio among the integrated emission intensities for glasses with a Ce:Si molar ratio of 1×10^{-3} was 2.2:1.0:22:30 for SG, BSG, PSG, and BPSG, respectively.

The room-temperature Ce^{3+} emission decay times (τ) for Ce-doped BSG and SG (Ce:Si molar ratio 1×10^{-3}) samples were 58 and 54 ns ($\lambda_{exc} = 290$ nm, $\lambda_{em} = 415$ nm), confirming that the environment of Ce^{3+} ions is similar in both host matrixes. Lower τ values ($\lambda_{exc} = 290$ nm) were found for the Ce-doped PSG and BPSG (Ce:Si = 1×10^{-3} molar ratio), 25 ns ($\lambda_{em} = 317$ nm) and 29 ns ($\lambda_{em} = 375$ nm), respectively. These values are very similar to those found for Ce^{3+} in phosphate glasses.[11,47]

Moreover, it is worth noting that the obtained emission decay times for the PSG and BPSG glasses do not vary notably on passing from the most Ce^{3+} diluted sample (Ce:Si = 1×10^{-4} molar ratio) to the most concentrated one (Ce:Si = 1×10^{-2} molar ratio). In fact, for the BPSG glasses the τ values range from 32 ns (Ce:Si = 1×10^{-4} molar ratio) to 29 ns (Ce:Si = 1×10^{-2} molar ratio), while for the PSG glasses the τ values range from 29 ns (Ce:Si = 1×10^{-4} molar ratio) to 25 ns (Ce:Si = 1×10^{-2} molar ratio). This behavior points to a negligible concentration quenching of the Ce^{3+} emission for the glasses under investigation in the present Ce:Si molar ratio range.

Luminescence results indicate that the presence of P in the glass network modifies the RE coordination environment with respect to SG and BSG and suggest that in PSG and BPSG Ce^{3+} ions preferentially interact with P-containing groups. The involvement of phosphorus in cerium coordination was also confirmed by the shift of the emission band to lower frequency with decreasing P:Ce atomic ratio. Even if the emission value still peaked in the Ce-doped phosphate region, for high Ce content the number of P units around RE decreased and probably caused the observed emission energy shift.

Electron Paramagnetic Resonance. The EPR analysis of the paramagnetic Ce^{3+} centers was performed at 4.2 K. In fact, no resonance lines were detected above 20 K, due to the rapid relaxation time T_1 which broadens the line width (line width $\propto T_1^{-1}$), as observed for most lanthanides[48] with the exception of S-state ions with a half-field subshell $4f^7$.

EPR spectra of Ce-doped SG showed a complex signal spanning about 10^4 G and consisting of several overlapped broad resonances (Figure 6a). The assignments of particular sets of lines to well-defined Ce^{3+} centers is not easy for the following reasons. The Ce^{3+} ground state is $^2F_{5/2}$, and the energy gap from the lowest excited state $^2F_{7/2}$ is 2250 cm^{-1}, owing to the spin−

(47) Das Mohapatra, G. K. *Phys. Chem. Glasses* **1998**, *39*, 50.
(48) Baker J. M. *EPR and ENDOR in the Lanthanides* in *Electron Spin Resonance*; The Royal Society of Chemistry: London, 1993; Vol. 13B, Chapter 3.

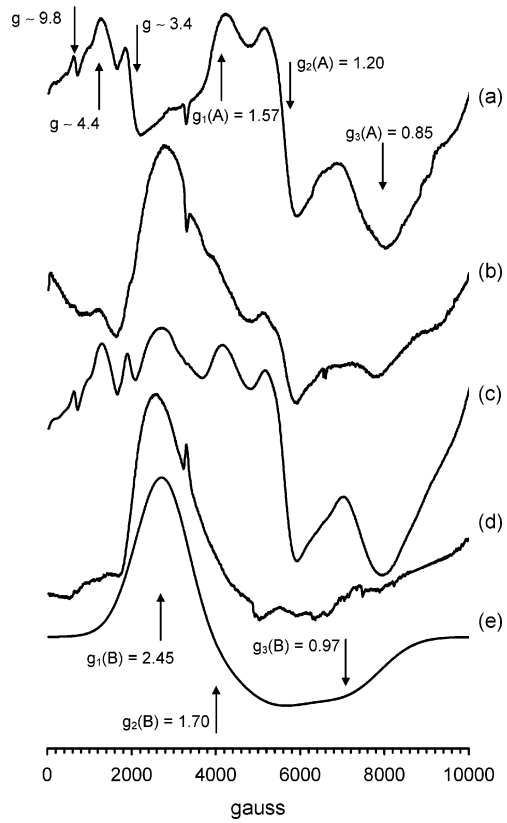

Figure 6. EPR spectra recorded at 4.2 K of (a) Ce-doped SG, (b) Ce-doped PSG, and (c) Ce-doped BPSG with a Ce:Si = 1×10^{-3} molar ratio. (d) Difference between normalized spectra (c) and (a). (e) Simulation of spectrum (d).

orbit coupling interaction. This excludes any significant contribution of the $^2F_{7/2}$ state in determining g values; on the contrary, the wave function of the $^2F_{5/2}$ ground state results, for a specific crystal field symmetry, from the linear combination of three Kramers doublets, which mixes the $|M_j = \pm 1/2\rangle$, $|M_j = \pm 3/2\rangle$, and $|M_j = \pm 5/2\rangle$ eigenfunctions.

Thus, the experimental **g** tensor values for Ce^{3+} in different symmetry fields depend on the mixing coefficients of the doublets[49−52] and can vary in a wide range of values, as reported in the large number of single-crystal studies.[53−60] In these crystal materials the intrinsic lattice defects (vacancies or substitutional ions) are the source of the distortion of the Ce^{3+} environment, especially when the RE ion charge differs from that of the substitutional site. When RE ions are incorporated into glasses, the behavior becomes even more complicated because the paramagnetic centers experience several and differently distorted symmetry fields, due to both amorphous matrix and structural defects.

To the best of our knowledge, no EPR study of Ce-doped glasses has been reported up to now. Notwithstanding, as the relative intensities of resonances at $g_1 = 1.57$, $g_2 = 1.20$, and $g_3 = 0.85$ (Figure 6a, signal A) in Ce-doped SG did not vary significantly for different cerium contents or by recording EPR spectra at 7.0 and 10.0 K (not shown spectra), signal A can be attributed to a single species, whose magnetic parameters are very similar to those reported by Yamaga et al.[57] for a Ce-doped $LiCaAlF_6$ single crystal.

The weaker lines at low magnetic field, ranging from $g \approx 10.5$ to $g \approx 3$ (Figure 6 a), are too overlapped to allow the **g** tensor components to be exactly evaluated. However, as the relative intensities of the three detectable lines at $g \approx 9.8$, $g \approx 4.4$, and $g \approx 3.4$ vary with both recording temperature and cerium content (spectra not shown), a single species was excluded. The values $g \approx 3.4$ and $g \approx 4.4$ are reminiscent of the g_{zz} components reported by Misra et al.[50,51] for Ce^{3+} ions in the orthorhombic crystal field of $CeBa_2Cu_3O_{7-\delta}$ and $CeBa_2Cu_4O_8$. According to this assignment, g_{xx} and g_{yy} values should range from 0.1 to 1.3, a region covered by the stronger lines of signal A.

The total intensity of Ce^{3+} resonances does not increase linearly with the cerium content. As an example, the signal area of the Ce:Si = 1×10^{-2} sample is about 1.5 times greater than that of the Ce:Si = 1×10^{-3} sample, despite a 10 times larger Ce content. Although it is not possible to calculate the absolute value of the Ce^{3+} amount from the EPR signal, due to the lack of suitable and significant quantitative standards, these data confirmed that part of the Ce^{3+} oxidized to Ce^{4+} and segregated as CeO_2.

The resonance lines of Ce-doped BSG (not shown) were similar to those of Ce-doped SG, but the intensity of the signals was about 1 order of magnitude lower in samples with the same cerium content. Taking into account that TEM micrographs of Ce-doped BSG showed the presence of CeO_2 nanoparticles only at a Ce:Si = 1×10^{-2} molar ratio, such low intensities can be ascribed to the oxidation of Ce^{3+} ions to Ce^{4+}, even in the absence of CeO_2 segregation, as observed by UV−vis spectroscopy.

When phosphorus was present, in both Ce-doped PSG and BPSG, a new anisotropic signal (signal B) overlapped the other resonances (Figure 6b,c). The intensity of signal B increased with the cerium content in both matrixes, but it was particularly evident in PSG glasses, where a lower contribution of signals A and B to the total resonance occurred. In BPSG, signal B was evidenced by subtracting the normalized EPR spectrum of Ce-doped SG from that of Ce-doped BPSG (Figure 6d). The spectrum was simulated by the values $g_1 = 2.45$, $g_2 = 1.70$, and $g_3 = 0.97$ (Figure 6e), similar to those reported by Misra and Isber[52] for Ce^{3+} in a $Y(NO_3)_3 \cdot 6H_2O$ single crystal. The presence of species B only in P-containing matrixes suggests that part of the Ce^{3+} ions are located in a different coordination environment, which involves phosphorus centers, in agreement with luminescence results.

The EPR investigation was also performed on X-ray-irradiated Ce-doped glasses. In a previous paper[37] we studied POHC I and II and BOHC paramagnetic defects, formed under X-ray

(49) Abragam, A.; Bleaney, B. *Electron Paramagnetic Resonance of Transition Metal Ions*; Clarendon Press: Oxford, 1970.
(50) Misra S. K.; Isber, S. *Physica B* **1998**, *253*, 111.
(51) Misra, S. K.; Chang, Y.; Felsteiner, J. *J. Phys. Chem. Solids* **1997**, *58*, 1.
(52) Yamaga, M.; Lee, D.; Henderson, B.; Han, T. P. J.; Gallagher, H. G.; Yosida, T. *J. Phys.: Condens. Matter* **1998**, *10*, 3223.
(53) Wingbermühle, J.; Meyer, M.; Schirmer, O. F.; Pankrath, R.; Kremer, R. K. *J. Phys.: Condens. Matter* **2000**, *12*, 4277.
(54) Asatryan, H. R.; Rosa, J.; Mareš, J. A. *Solid State Commun.* **1997**, *104*, 5.
(55) Yosida, T.; Yamaga, M.; Lee, D.; Han, T. P. J.; Gallagher, H. G.; Henderson, B. *J. Phys.: Condens. Matter* **1997**, *9*, 3733.
(56) Yamaga, M.; Kodama, N.; Yosida, Y.; Henderson, B.; Kindo, K. *J. Phys.: Condens. Matter* **1997**, *9*, 9639.
(57) Yamaga, M.; Honda, M.; Shimamura, K.; Fukuda, T.; Yonda, T. *J. Phys.: Condens. Matter* **2000**, *12*, 5917.
(58) Yamaga, M.; Honda, M.; Kawamata, N.; Fujita, T.; Shimamura, K.; Fukuda, T. *J. Phys.: Condens. Matter* **2001**, *13*, 3461.
(59) Yamaga, M.; Hattori, K.; Kodama, N.; Ishizawa, N.; Honda, M.; Shimamura, K.; Fukuda, T. *J. Phys.: Condens. Matter* **2001**, *13*, 10811.
(60) Misra, S. K.; Andronenko, S. I. *J. Phys. Chem. B* **2004**, *108*, 9397.

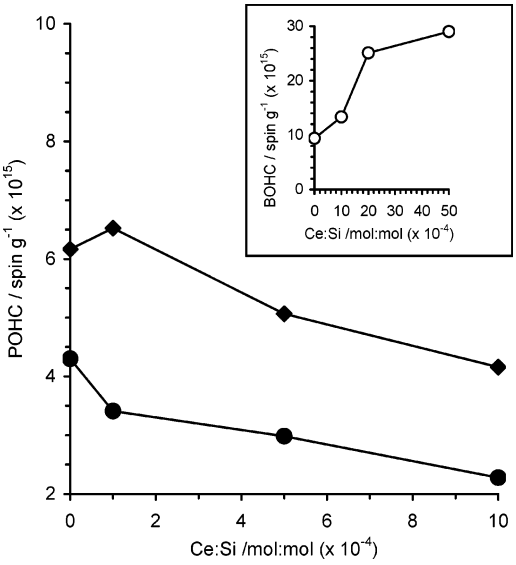

Figure 7. Amount of POHC defects vs Ce content in X-ray-irradiated Ce-doped PSG (●) and BPSG (◆). Inset: amount of BOHC defects vs Ce content in X-ray-irradiated Ce-doped BSG.

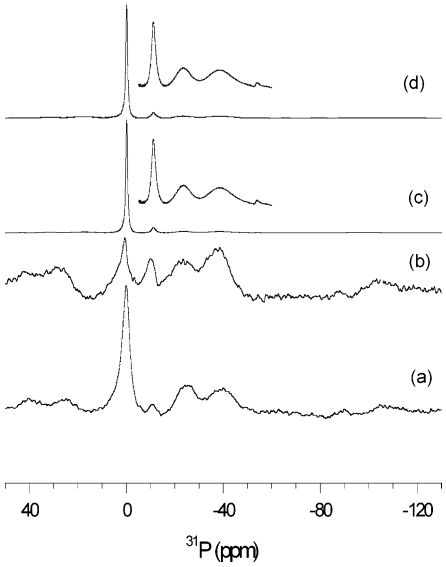

Figure 8. ^{31}P MAS NMR spectra of (a) undoped PSG, (b) undoped BPSG, (c) Ce-doped PSG, and (d) Ce-doped BPSG with a Ce:Si = 1×10^{-3} molar ratio.

irradiation of undoped PSG, BSG, and BPSG. The majority POHC I center was modeled as a hole (h^+) shared between two oxygen atoms, both in a nonbridging configuration[61] and in one where one atom is bridging and the other one not;[62] the minor component POHC II was associated with one h^+ located on a single nonbridging oxygen atom.[61] According to these hypotheses, their diamagnetic precursors could be metaphosphate, $[O{=}PO_{2/2}O]^-$, or phosphoryl, $[O{=}PO_{3/2}]$, units, linked to the silica network via bridging oxygens.[61,62] BOHC was described as one h^+ trapped by a bridging oxygen in the Si−O−B linkage, where B is located in a tetrahedral boron unit, $[BO_{4/2}]^-$;[63] more recently, it was modeled as one h^+ located on a nonbridging oxygen, >B−O•, originated from a trigonal boron unit, $[BO_{3/2}]$.[64] In undoped BSG and PSG the number of these defects increased with B and P content, but in BPSG the copresence of both doping elements improved the formation yield of POHCs I and II, with respect to PSG, the P content being equal, and strongly decreased the BOHC amount with respect to BSG.[37]

Comparing the X-ray-irradiated Ce-doped PSG and BPSG, the amount of POHC was still higher in ternary glasses but decreased with increasing cerium content for both matrixes (Figure 7). This behavior suggests that part of the POHC diamagnetic precursors interacted with RE ions, thus lowering the number of h^+ traps. BOHC defects had different behavior; in fact, the number of BOHC defects, which was very low in Ce-doped BPSG as in undoped BPSG, increased with the RE concentration in Ce-doped BSG (inset in Figure 7). This excluded any direct interaction between cerium and the BOHC precursor.

Magic Angle Spinning Nuclear Magnetic Resonance. Undoped and Ce-doped (Ce:Si = 1×10^{-3} molar ratio) BSG, PSG, and BPSG were investigated by ^{31}P, ^{29}Si, and ^{11}B MAS NMR to study the glass structural modifications induced by the RE addition.

(a) ^{31}P MAS NMR. The ^{31}P MAS NMR spectrum of PSG showed four signals (Figure 8a). Two quite large resonances, with similar intensities, peaking at about −25 ppm (fwhm = 10.2 ppm, ∼29%) and −39 ppm (fwhm = 6.9 ppm, ∼32%) were attributed, respectively, to metaphosphate, $[O{=}PO_{2/2}O]^-$, and phosphoryl, $[O{=}PO_{3/2}]$, groups, where two and three oxygen atoms bridge other glass tetrahedral units.[65,66] The less intense third resonance at −10.7 ppm (fwhm = 2.9 ppm, ∼2%) is due to pyrophosphate, $[O{=}PO_{1/2}O_2]^{2-}$, species, where one oxygen atom bridges one tetrahedral unit. The presence of sidebands of these resonances suggests that the cross-linked phosphorus is held rigidly. The strong signal at about 0 ppm was attributed to orthophosphate, $[PO_4]^{3-}$, species (fwhm = 3 ppm, ∼37%); orthophosphate groups were roughly one-third of the total phosphorus, and their narrow lines are indicative of a high degree of mobility despite the solid appearance of glass.

The addition of B (BPSG) did not modify the number of signals and their chemical shifts and fwhm, but caused very significant changes in the relative amount of the different species (Figure 8b). A large decrease of orthophosphate and pyrophosphate species (<10%) was observed. Also metaphosphate groups (16%) decreased, while a large increase of phosphoryl groups (74%) occurred. This indicates that phosphorus-containing units became more condensed to the silica network with respect to PSG. No evidence of direct interaction between boron and phosphorus was found; in fact, boron atoms bonded to branched phosphorus units (Q_3) should show up at about −30 ppm and boron atoms bonded to middle phosphate units (Q_2) at about −5 and −10 ppm.[67] According to this, the higher number of POHC paramagnetic defects observed in ternary glasses[37,62] can be associated with the large increase of $[O{=}PO_{3/2}]$ groups,

(61) Griscom, D. L.; Friebele, E. J.; Long, K. J.; Fleming, J. W. *J. Appl. Phys.* **1983**, *54*, 3743−3761.
(62) Warren, W. L.; Shaneyfelt, M. R.; Fleetwood, D. M.; Winokur, P. S. *Appl. Phys. Lett.* **1995**, *67*, 995−997.
(63) Griscom, D. L.; Sigel, G. H.; Ginther J. *J. Appl. Phys.* **1976**, *47*, 960−967.
(64) Shkrob, I. A.; Tarasov, V. F. *J. Chem. Phys.* **2000**, 10723−10732.
(65) Hartmann, P.; Vogel, J.; Schnabel, B. *J. Non-Cryst. Solids* **1994**, *176*, 157−163.
(66) Szu, S. P.; Klein, L. C.; Greenblatt, M. *J. Non-Cryst. Solids* **1992**, *143*, 21−30 and references therein.
(67) Ducel, J. F.; Videau, J. J.; Suh, K. S.; Senegas, J. *Phys. Chem. Glasses* **1994**, *35*, 10−16.
(68) Fanciulli, F.; Bonera, E.; Carollo, E.; Canotti, L. *Microelectron. Eng.* **2001**, *55*, 65−71.
(69) Carboni, R.; Pacchioni, G.; Fanciulli, M.; Giglia, A.; Mahne, N.; Pedio, M.; Nannarone, S.; Boscherini, F. *Appl. Phys. Lett.* **2003**, *83*, 4312.

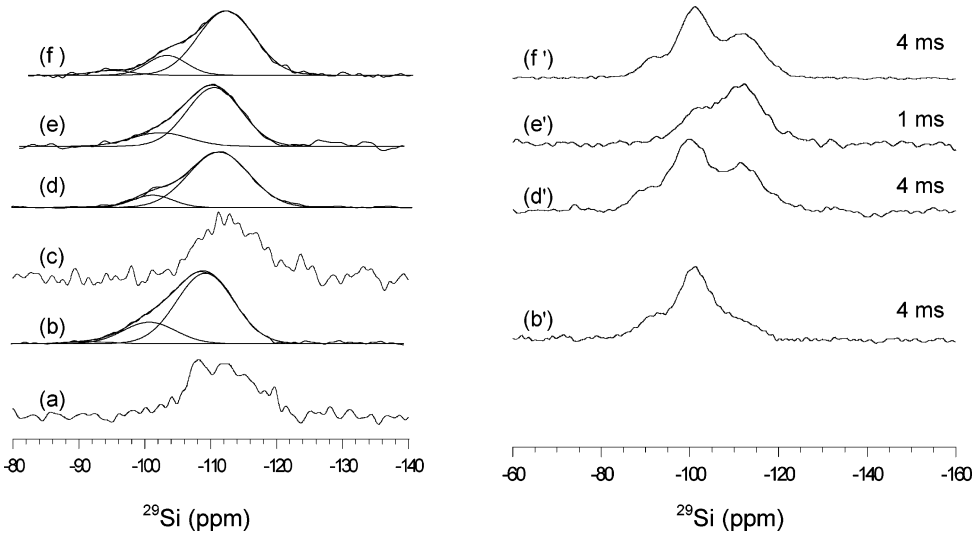

Figure 9. ^{29}Si MAS NMR (left) and CP MAS NMR (right) spectra of (a) undoped PSG, (b, b′) undoped BSG, (c) undoped BPSG, (d, d′) Ce-doped PSG, (e, e′) Ce-doped BSG, and (f, f′) Ce-doped BPSG with a Ce:Si = 1×10^{-3} molar ratio. The contact times are reported next to the relative CP MAS NMR spectra.

which may be identified as the most plausible POHC precursors in agreement with Warren et al.[62] On the contrary, these results did not support the suggestion that B and P codoping decreases the number of P═O groups.[68,69]

Ce-doped PSG and BPSG spectra showed the same number of resonances as undoped PSG and BPSG spectra (Figure 8c,d). Both spectra were dominated by the orthophosphate resonances at 0 ppm (respectively ∼63% and ∼71%); the lines were narrower than in PSG and BPSG, indicating a high increase of the orthophosphate mobility. The pyrophosphate amount slightly increased (∼10% and ∼6%) while those of phosphoryl (∼16% and ∼14%) and metaphosphate (∼11% and ∼ 9%) strongly decreased, when compared to those of undoped glass. This is indicative of a remarkably lower cross-linking between the phosphorus units and the silica network as a consequence of the presence of cerium, which acts as a network modifier, and hampers the formation of P−O−Si bridges. The decrease of POHC defects with increasing cerium content for both PSG and BPSG matrixes (Figure 7) agrees with the large decrease of their diamagnetic precursors [O═$PO_{3/2}$] in the presence of RE ions.

(b) ^{29}Si MAS and CPMAS NMR. The ^{29}Si MAS NMR spectrum of PSG showed an asymmetric shape with a very low signal:noise ratio (Figure 9a). The sample was non-cross-polarizable, ruling out the presence of hydroxyl groups. The chemical shift value, obtained by signal deconvolution with a single Gaussian curve, was about -111.3 ± 0.2 ppm with fwhm $\approx$ 10 ppm and was attributed to Q_4 species according to the literature (Q_n stands for a SiO_4 tetrahedron of the amorphous network, which forms n bonds with neighboring tetrahedra).[70] The chemical shift value was slightly different from that observed in sol−gel-prepared silica glasses (∼−110 ppm).[71] Although more negative values should be expected when silicon is replaced by phosphorus,[72−74] the line asymmetry and broadening might hinder the detection of a more significant shielding. Therefore, Si−O−P bond formation, evidenced by the ^{31}P resonances at −23 and −39 ppm, was undetectable, though not ruled out, by the ^{29}Si spectrum.

The ^{29}Si MAS NMR spectrum of BSG has a different pattern compared to that of PSG. It showed an asymmetric shape at low frequency, suggesting the presence of overlapped Q_n signals (Figure 9b): in addition to Q_4 (-110.0 ± 0.1 ppm), two other signals attributed to the less condensed Q_3 (-101.0 ± 0.2 ppm) and Q_2 (-92.0 ± 0.2 ppm) groups became evident. The Q_n distribution was obtained by nonlinear fitting of the MAS NMR spectra with individual Gaussians. The calculated line widths and integrated areas are for Q_4 (fwhm = 8.7 ± 0.3 ppm, 77%), Q_3 (fwhm = 8.0 ± 0.2 ppm, 21%), and Q_2 (fwhm = 7.1 ± 0.2 ppm, 2%). The sample was cross-polarizable (Figure 9b′). The cross-polarization (CP) spectra are not quantitative as the CP technique generates signals from the silicon atoms that are dipolar-coupled to hydrogen, and since the signal response decreases rapidly with increasing distance from hydrogen atoms, the relative intensities of the Q_n resonances become weaker as n increases. In particular, Q_4 signals can be only due to SiO_4 tetrahedra close to noncontinuous network zones in the glass matrix where OH groups are located. The chemical shift values observed in BSG were in the range of pure silica, although it was expected[75] that the Si−O−BO_2 linkage, with trigonal boron-centered units, should cause a chemical shift similar to that of a Si−O−Si bond, whereas the Si−O−BO_3 linkage, with tetrahedral units, should cause deshielding with respect to Si−O−Si. Therefore, on the basis of ^{29}Si results, Si−O−B interaction was undetectable, probably due to the low boron concentration (due to a ∼30% loss of the total B amount during glass formation).

The ^{29}Si MAS NMR spectrum of BPSG (Figure 9c) shows a very low signal:noise ratio and a broad more shielded side than that observed in PSG spectrum. The sample is non-cross-

(70) Lippmaa, E.; Magi, M.; Samoson, A.; Enghelhardt, G.; Grimmer, A. R. *J. Am. Chem. Soc.* **1980**, *102*, 4889.
(71) Engelhardt, G. *High Resolution Slolid State NMR of Silicates and Zeolites*; Wiley: New York, 1987.
(72) Lockyer, M. W.; Holland, D.; Dupree, R. *Phys. Chem. Glasse* **1995**, *36*, 22.
(73) Schramm, C. M.; de Jong, B. H. W. S.; Parziale, V. E. *J. Am. Chem. Soc.* **1984**, *106*, 4396.
(74) Grimmer, A. R.; Magi, M.; Hahnert, M.; Stade, H.; Samoson, A.; Wieker, W.; Lippmaa, E. *Phys. Chem. Glasses* **1984**, *25*, 105.
(75) Bunker, B. C.; Tallant, D. R.; Kirkpatrick, R. J.; Turner, G. L. *Phys. Chem. Glasses* **1990**, *31*, 30−41.

polarizable, ruling out the presence of hydroxyl groups. The resonance lines were fitted by a single Gaussian (-113 ± 0.2 ppm, fwhm $\approx$ 9.7 ppm) and show significant shielding, indicating an increase of the cross-linking between silica and phosphate units, in good agreement with the data of the ^{31}P MAS spectrum.

The ^{29}Si MAS NMR spectra of Ce-doped PSG, BSG, and BPSG showed in general different patterns compared to those of undoped samples (Figure 9d−f), suggesting that Ce atoms inhibit the silica condensation process. In fact, MAS spectra of Ce-doped PSG and BPSG samples showed three overlapped Q_n signals which can be deconvolved in three Gaussian lines and were cross-polarizable (Figure 9d′−f′). The Q_n distribution for PSG is Q_4 (-110.2 ± 0.2 ppm, fwhm = 9.1+0.1 ppm, 84%), Q_3 (-101.2 ± 0.2 ppm, fwhm = 6.4 ± 0.2 ppm, 15%), and Q_2 (-92.0 ± 0.2 ppm, fwhm = 5.9 ± 0.2 ppm, 1%). For BPSG the distribution is Q_4 (-110.5 ± 0.2 ppm, fwhm = 8.7 ± 0.1 ppm, 79%), Q_3 (-101.0 ± 0.2 ppm, fwhm = 7.1+0.1 ppm, 18%), and Q_2 (-92.0 ± 0.2 ppm, fwhm = 6.0 ± 0.1 ppm, 3%). No evidence of Si−O−B bonds nor cross-linking between the SiO_4 and PO_4 units was observed. The spectrum of Ce-doped BSG appears asymmetric (Figure 9e) and broader on the less shielding side. It can be deconvolved in two Gaussian lines: Q_4 (-110.4 ± 0.1 ppm, fwhm = $8.5.0 \pm 0.2$ ppm, 83%) and Q_3 (-102.0 ± 0.2 ppm, fwhm = 7.7 ± 0.1 ppm, 17%). Unlike pure BSG and Ce-doped PSG and BPSG, this sample was non-cross-polarizable with a 4 ms contact time, a typical value for the maximum polarization of silica.[76] When the CP spectra were collected with a 1 ms contact time, two overlapping signals, Q_3 (103.0 $\pm$ 0.1 ppm) and Q_4 (110.0 $\pm$ 0.1 ppm), occurred (Figure 9e′). The observed loss of cross-polarizable signal at a 4 ms contact time in the presence of cerium can be ascribed to the effect of paramagnetic Ce^{3+}. The efficiency of the magnetization transfer from ^{1}H nuclei to Si nuclei is governed by the characteristic proton spin−lattice relaxation time in the rotating frame ($T_{1\rho}$) and the silicon−proton cross-polarization time (T_{SiH}).[77,78] It may be suggested that in BSG, Ce^{3+} centers lying near silanol groups induce the $T_1\rho$ relaxation process of protons via paramagnetic centers, limiting the polarization transfer to silicon centers. In PSG and BPSG, where Ce^{3+} preferentially interacts with P centered units, the polarization transfer to silicon occurs even at 4 ms contact time.

(c) ^{11}B MAS NMR. The ^{11}B MAS NMR spectra of undoped BSG and BPSG and Ce-doped BSG and BPSG are shown in Figure 10. The broad signals ranging from about 0 to 25 ppm were attributed to $[BO_{3/2}]$ units, while the sharp signals at lower chemical shift arise from $[BO_{4/2}]^-$ units.[79,80]

Unfortunately ^{11}B MAS NMR experiments, performed at low or intermediate magnetic fields (<10 T), suffer for the heavy overlap of resonances due to different $[BO_{3/2}]$ sites and of those due to $[BO_{3/2}]$ and $[BO_{4/2}]^-$ contributions, which require mathematically complicated best fit procedures to evaluate the quadrupolar parameters.

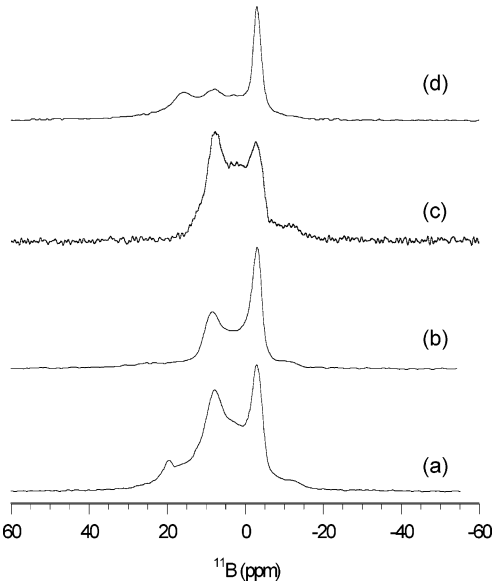

Figure 10. ^{11}B MAS NMR spectra of (a) undoped BSG, (b) undoped BPSG, (c) Ce-doped BSG, and (d) Ce-doped BPSG with a Ce:Si = 1×10^{-3} molar ratio.

Table 1. NMR Parameters Used for Curve Fitting of ^{11}B MAS Spectra

	δ_{iso} (ppm)	%	C_Q (MHz)	η
		BSG		
$[BO_{3/2}]$	24.0 ± 0.2	17 ± 4	2.6 ± 0.1	0.1
	13.0 ± 0.1	49 ± 2	2.6 ± 0.1	0.2
	16.4 ± 0.3	22 ± 3	2.5 ± 0.1	0.2
$[BO_{4/2}]^-$	-3.0 ± 0.1	12 ± 4	0.3 ± 0.1	0.0
		BPSG		
$[BO_{3/2}]$	11.8	72	2.5	0.2
$[BO_{4/2}]^-$	−4.3	28	0.3	0.0
		Ce−BSG		
$[BO_{3/2}]$	12.6	73	2.7	0.2
	16.7	27	2.7	0.2

The relative abundance of the boron species was here calculated by fitting the spectra with the WSOLIDS software.[39] Published data on quadrupolar parameters ($C_Q = e^2qQ/h$) and asymmetry parameters (η) provided constraints on the $[BO_{3/2}]$ and $[BO_{4/2}]^-$ peak shapes.[79−84] The results of the fitting procedure for undoped and doped BSG and BPSG are reported in Table 1. Although they cannot be considered to be highly accurate, due to the strong signal overlap, they nonetheless allow a comparison among the different samples.

The ^{11}B MAS spectrum of BSG (Figure 10a) is dominated by the signals of three $[BO_{3/2}]$ units (total amount 88%) at δ_{iso} = 24, 16.4, and 13.0 ppm (Table 1). The two peaks at δ_{iso} = 13.0 and 16.4 ppm can be attributed to $[BO_{3/2}]$ sites in the borosilicate glass network.[79−82] Although a precise peak assignment is not straightforward, an upfield shift of several parts per million from 19 ppm (peak position for boric acid or borate glass) is expected when silicon (rather than boron or hydrogen) is the next nearest neighbor of the boron atom. This suggests that the signal at δ_{iso} = 13.0 ppm could be assigned to $[BO_{3/2}]$

(76) Leonardelli, S.; Facchini L.; Fretigny C.; Tougne P.; Legrand, A. P. *J. Am. Chem. Soc.* **1992**, *114*, 6412.
(77) Mehring, M. *Principles of High Resolution NMR in Solids*, 2nd ed.; Springer-Verlag: New York, 1983.
(78) Slichter, C. P. *Principles of Magnetic Resonance*, 3rd ed.; Springer-Verlag: New York, 1989.
(79) van Wullen L.; Muller-Walmuth, W. *Solid State Nucl. Magn. Reson*. **1993**, *2*, 279−284.
(80) Martens, R.; Muller-Warmuth, W. *J. Non-Cryst. Solids* **2000**, *265*, 167−175.
(81) Irwin, A. D.; Holmgren, J. S.; Jonas, J. *J. Non-Cryst. Solids* **1988**, *101*, 249−254.
(82) van Wullen, L.; Muller-Walmuth, W.; Papageorgiou, D.; Pentinghaus, H. G. *J. Non-Cryst. Solids* **1994**, *171*, 53.
(83) Zuchner, L.; Chan, J. C. C.; Muller-Walmuth, W.; Eckert, E. *J. Phys. Chem. B* **1998**, *102*, 4495.
(84) Lin-Shu Du; Stebbins J. F. *J. Non-Cryst. Solids* **2003**, *315*, 239−255.

units connected with three SiO_4 tetrahedra, $[B(OSi)_3]$. The signal at $\delta_{iso} = 16.4$ ppm can be assigned to boroxol rings within a borate type of network.[80,82,85] The third peak at 24 ppm, an apparent singlet at lower field than the main peaks, can be assigned to boron in an asymmetric trigonal environment.[81,86] In addition to $[BO_{3/2}]$ signals, the peak at -3.0 ppm was attributed to boron in a tetrahedral $[BO_{4/2}]^-$ environment. The above results indicate that in BSG boron atoms are not homogeneously distributed as in a borosilicate glass phase, but borate-like zones, where $[BO_{3/2}]$ units are linked together, also occur.

The BPSG spectrum showed a clear increase of the $[BO_{4/2}]^-$ sites (28%) with respect to $[BO_{3/2}]$ (72%) (Figure 10b). Only one type of $[BO_{3/2}]$ site was observed at $\delta_{iso} = 11.8$ ppm and assigned to boron atoms in a borosilicate glass phase. Considering that the BOHC amount decreased from BSG to BPSG,[37] ^{11}B MAS NMR spectra suggest $[BO_{3/2}]$ as the most plausible BOHC precursor, in agreement with the Shkrob hypothesis.[64]

The addition of cerium affects boron units in the BSG or BPSG host in different ways. In Ce-doped BSG (Figure 10c), two peaks at $\delta_{iso} = 12.6$ and 16.7 ppm assigned to $[BO_{3/2}]$ units showed up, but the number of $[BO_{4/2}]^-$ units strongly decreased. Moreover, the main peak at 12.6 ppm (73%) was slightly high field shifted compared to that observed in undoped BSG, suggesting that boron and silicon are more cross-linked in the doped glass. The Ce-doped BPSG spectrum (Figure 10d) appeared less structured if compared to the three other ^{11}B spectra. At least three main peaks can be distinguished. The two peaks at 18.0 and 8.3 ppm were attributed to $[BO_{3/2}]$ units; specifically, the latter small peak at 8.3 ppm was a clear indication of lower cross-linking between $[BO_{3/2}]$ and silica. The peak at -3.4 ppm was attributed to $[BO_{4/2}]^-$ sites, whose amount increased with respect to undoped BPSG. The relevant amount of $[BO_{3/2}]$ units in Ce-doped BSG together with the increase of BOHC with cerium content (inset in Figure 7) confirms $[BO_{3/2}]$ units as more probable BOHC precursors.

Concluding Remarks

The luminescence properties of cerium in silica-based glasses are strongly affected by the presence of B and P former elements. In P-containing glasses, PSG and BPSG, the emission yield is strongly enhanced, unlike in BSG where B alone does not improve the luminescence properties. The oxidation of Ce^{3+} to Ce^{4+} and the segregation of CeO_2 seem to be the main processes responsible for the luminescence yield variations; therefore, in the following, we discuss on this basis the reasons why the RE electronic state depends on the B and P doping elements.

(i) HRTEM micrographs showed that, in Ce-doped SG, CeO_2 segregates at very low Ce:Si molar ratio, 5×10^{-4}. The inclusion of B and P in silica precludes the segregation of CeO_2 up to Ce:Si $= 1 \times 10^{-2}$ in all matrixes, BSG, PSG, and BPSG. This is probably due to B and P centers which induce the formation of $[BO_{4/2}]^-$, $[O{=}PO_{2/2}O]^-$, $[O{=}PO_{3/2}]$, $[O{=}PO_{1/2}O_2]^{2-}$, and $[OPO_3]^{3-}$ units. Their negative charge and/or nonbridging oxygen atoms make the glass matrix more suitable to embed RE ions without CeO_2 segregation. Nevertheless, if the Ce emission yield is affected only by CeO_2 segregation, no significant differences should be expected among BSG, PSG, and BPSG matrixes. The presence of a very intense charge-transfer band in SG and BSG UV−vis absorption spectra assigned to Ce^{4+} demonstrates that diluted Ce^{4+} centers are stable also in the absence of CeO_2, resulting in a lower luminescence yield. The higher stability of the upper oxidation state Ce^{4+} in SG and BSG with respect to phosphate-containing glasses PSG and BPSG agrees with the behavior suggested by the optical basicity model.[87,88]

(ii) The results of MAS NMR investigation showed that the phosphorus units in PSG and BPSG were phosphoryl, $[O{=}PO_{3/2}]$ (Q_3), metaphosphate, $[O{=}PO_{2/2}O]^-$ (Q_2), pyrophosphate, $[O{=}PO_{1/2}O_2]^{2-}$ (Q_1), and orthophosphate, $[PO_4]^{3-}$ (Q_0). All phosphate units are able to coordinate RE centers,[89] the interaction being strengthened by the charge polarization of the $P^{\delta+}{=}O^{\delta-}$ group. On the basis of the ^{31}P chemical shift values, the bond strength should follow the order $Q_3 > Q_2 > Q_1 > Q_0$; this suggests that Q_3 and Q_2 coordinate the RE ions, even if the contribution of the minor component Q_1 cannot be excluded. The high mobility of Q_0 indicates that these groups did not interact with RE ions, despite their large number in Ce-doped glasses. The coordination with the P-containing units causes an electron transfer from the $P^{\delta+}{=}O^{\delta-}$ group to Ce^{3+} and enhances the stability of Ce^{3+}, hindering both the oxidation to Ce^{4+} and the segregation of CeO_2.

Neither trigonal nor tetrahedral boron centers are involved in RE coordination. In $[BO_{3/2}]$ units, B is electron deficient. On the other hand, $[BO_{4/2}]^-$ units do not contain any nonbridging oxygen, and their negative charge is spread over the whole BO_4 group.[90] This explains the high amount of dispersed Ce^{4+} centers in BSG.

(iii) The stabilization of Ce^{3+} due to RE interaction with P=O is also supported by EPR results. In fact, a new Ce^{3+} species, B, with a different RE coordination environment with respect to that of the species found in SG and BSG, was observed in PSG and BPSG. The decrease of the POHC number with cerium content further confirmed the RE interaction with P-related defects; in fact, the ability of phosphoryl, $[O{=}PO_{3/2}]$, units, diamagnetic precursors of the POHC defects, to trap electronic holes under X-ray irradiation decreases by interaction with Ce^{3+} ions.

(iv) The Ce^{3+} photoluminescence emission band in PSG and BPSG matrixes peaked at 330−340 nm, a range very similar to that of Ce^{3+} in pure phosphate glasses,[11,41] and at the same time, the emission energy in BSG samples peaked at 410 nm, quite similar to that in SG. This confirms the RE interaction with P=O groups in P-containing glass matrixes. The shift to lower energy of the Ce^{3+} emission band for a Ce:Si $\geq 5 \times 10^{-3}$ molar ratio could be explained by assuming a progressive modification of RE coordination with increasing RE concentration. As the value of the P:Ce molar ratio decreases to a value

(85) Joo C.; Werner-Zwanzigher U.; Zwanzigher J. W. *Phys. Chem. Glasses* **2000**, *41*, 317.
(86) Kroeker S.; Stebbins J. F. *Inorg. Chem.* **2001**, *40*, 6239−6246.
(87) Duffy, J. A.; Ingram, M. D. *J. Non-Cryst. Solids* **1976**, *21*, 373.
(88) Duffy, G. A. *J. Non-Cryst. Solids* **1996**, *196*, 45.
(89) Hart, F. A. Scandium, Yttrium and Lanthanides. In *Comprehensive Coordination Chemistry*; Wilkinson, J., Gillard, R. D., McClaverty J., Eds.; Pergamon Press: Oxford, U.K., 1987; Vol. 6, Chapter 39.
(90) Rao, K. J. *Structural Chemistry of Glasses*; Elsevier Science: Oxford, U.K., 2002; Chapter 12 and references therein.

comparable with the real coordination numbers 6−8 of Ce^{3+} in metaphosphate glasses,[91] the coordination shell involves an increasing number of $Si-O^-$ groups and originates Ce^{3+} sites with lower emission energy.

(91) Bowron, D. T.; Saunders, G. A.; Newport, R. J.; Rainford, B. D.; Senin, H. B. *Phys. Rev. B* **1996**, *53*, 5268.

Acknowledgment. We thank MIUR (PRIN 2003) for financial support.

Supporting Information Available: Complete ref 5. This material is available free of charge via the Internet at http://pubs.acs.org.

JA052502O